Electrical Power and Energy Systems 181 (2026) 112092

Contents lists available at ScienceDirect

International Journal of Electrical Power and Energy Systems

journal homepage: www.elsevier.com/locate/ijepes

Stochastic capacity expansion planning with flexible demand: A progressive hedging approach

Yuting Mou *, Abdullah

School of Electrical Engineering, Southeast University, Nanjing 210018, Jiangsu Province, China

ARTICLE INFO

Keywords:
Capacity expansion planning
Mixed-integer programming
Flexible demand
Stochastic optimization
Demand-side management
Progressive hedging

ABSTRACT

Power systems in many developing economies face persistent supply deficits that are typically managed through undifferentiated load shedding. This approach ignores the diverse flexibility characteristics across consumer categories, imposing avoidable economic costs that a more targeted strategy could reduce. This paper proposes a two-stage stochastic capacity expansion planning model that co-optimizes generation investment, independently sized battery power and energy capacities, flexible electric vehicle charging, and binary scheduling of industrial demand-side management under demand and electric vehicle penetration uncertainties. The first stage determines new generation and storage capacities, while the second stage optimizes hourly dispatch, storage operation, and maintenance and work-shift curtailment schedules for industrial consumers. System reliability risk is addressed through a Conditional Value-at-Risk measure on energy not served. The resulting large-scale mixed-integer linear program is solved via Progressive Hedging decomposition, with the load-shedding risk level treated as a first-stage consensus variable to preserve scenario separability. Case studies based on the Pakistani power system show that the stochastic model reduces total expected cost by 1.84% compared to its deterministic counterpart, coordinated demand-side flexibility lowers system cost by 1.04% relative to the inflexible baseline, and the Progressive Hedging algorithm converges within 31 iterations for instances with over 1.4 million binary variables. These results indicate that integrating demand-side flexibility into stochastic capacity planning is an effective risk-aware strategy for deferring generation investment while preserving reliability in supply-constrained systems.

1. Introduction

1.1. Background

Electricity shortages and routine load shedding remain persistent problems in many developing economies, where demand consistently exceeds the generation capacity that can be reliably dispatched. In Pakistan, a combination of rapid demand growth, chronic under-investment in generation, and heavy dependence on expensive imported fuels has produced prolonged and frequent load shedding with significant economic and social consequences [1]. Similar structural power deficits and their economic consequences have been documented in Nepal [2] and Brazil [3]. The conventional response is rolling blackouts, in which distribution feeders are disconnected sequentially for fixed durations regardless of the economic value of supply to different consumer categories [4]. Many consumers, however, display diverse flexibility characteristics that rolling blackouts do not exploit. For instance, some industries can shift annual maintenance shutdowns to periods of power shortage, while factories can reschedule weekly work-shift off-days at comparatively low cost [5]. Coordinated demand-side management (DSM) that accounts for these consumer-specific scheduling constraints can reduce involuntary curtailment relative to uniform rationing [6], which serves as an attractive short-term solution. Addressing the shortage over the long term, however, cannot rely on demand-side coordination alone. Instead it also requires well-planned investment in new generation and storage capacity, so that demand flexibility and capacity expansion are considered jointly rather than in isolation.

This joint problem is naturally formulated as a capacity expansion planning (CEP) problem with DSM. In conventional CEP frameworks, electricity demand is typically treated as an exogenous fixed parameter, yet the uncertainties in future demand undermine the reliability of deterministic planning approaches [7]. Such uncertainty admits two complementary remedies, i.e., improving the forecasts that feed the planning model, for example through modern deep-learning predictors such as long short-term memory networks enhanced with attention mechanisms [8], and explicitly embedding the uncertainty

* Corresponding author.
E-mail addresses: yutingmou@seu.edu.cn (Y. Mou), 223247096@seu.edu.cn (Abdullah).

https://doi.org/10.1016/j.ijepes.2026.112092
Received 29 April 2026; Received in revised form 12 July 2026; Accepted 28 July 2026

within the optimization through risk-aware stochastic formulations [9], and this paper follows the latter route. Pakistan's combination of an acute supply deficit, a large industrial demand base, rising EV penetration, and an undifferentiated rationing practice is therefore treated as a representative case which provides a well-motivated setting for a planning framework that jointly optimizes generation investment and consumer-specific scheduling [10].

1.2. Literature review

1.2.1. Generation capacity expansion modeling approach

Generation capacity expansion planning has been studied extensively over the past decades, evolving from early deterministic formulations optimized against fixed demand forecasts toward two-stage stochastic programming frameworks that separate irreversible first-stage investment decisions from recourse operational decisions evaluated across uncertainty realizations. For instance, Ref. [11] applies stochastic dynamic programming to generation expansion under hydro uncertainty, establishing that explicitly modeling uncertainty leads to materially different and less costly portfolios than deterministic solutions. This is extended to market-based settings in [7], formulating a two-stage stochastic problem that captures uncertainties in both demand growth and electricity prices. The two-stage stochastic programming framework, reviewed in [12], remains the dominant modeling paradigm for CEP, where the first-stage investment decisions are made before uncertainty is resolved, while second-stage operating decisions adapt to each realized scenario. More recent work has addressed additional complexity, including Ref. [9], which incorporates climate mitigation scenarios into a risk-balancing expansion model, showing that ignoring long-term policy uncertainty can substantially distort investment priorities. Ref. [13] provides a comprehensive review of optimization models for power system expansion, highlighting that most existing models treat either storage, demand response, or generation investment in isolation, and that jointly modeling these components under uncertainty remains an open research problem.

1.2.2. Battery energy storage systems in capacity expansion

Battery energy storage systems (BESS) have received growing attention as a means of integrating variable renewables and deferring investment in conventional peaking capacity. Ref. [14] shows that co-optimizing grid-scale storage investment alongside generation planning yields noticeably higher economic value than treating storage as an afterthought, particularly when renewable penetration is high. More recently, Ref. [15] develops a capacity expansion model that co-optimizes conventional generation, renewables, and long-term energy storage to assess how a capacity market mechanism affects investment and reliability under high renewable penetration, finding that long-term storage alone is insufficient to ensure adequacy without complementary firm capacity, while Ref. [16] also co-optimizes storage investment with network expansion under both long- and short-term uncertainties, confirming the growing planning value of storage under uncertainty. A distinguishing feature of BESS planning, compared with conventional generation, is that power conversion system (PCS) capacity and battery energy capacity must be optimized separately, since storage duration is itself a decision variable rather than a fixed technical parameter. Incorporating BESS into large-scale stochastic planning problems introduces increased computational difficulty, because state-of-charge dynamics couple operational decisions across consecutive time periods, which is addressed in [17] by applying a progressive hedging decomposition to the joint problem of battery sizing, siting, and dispatch, using temporal coupling of state-of-charge variables across scenario boundaries. The present work adopts a similar decomposition philosophy for the Pakistan system, extending it to include joint optimization of generation investment, BESS sizing, and demand-side management.

1.2.3. Demand side management in capacity expansion

In the context of capacity expansion, DSM can reduce the need for new peaking plant by making existing capacity more productive. As demonstrated in [6], even modest DSM participation can materially reduce the required generation investment by flattening peak demand, while Ref. [18] shows that demand response programs, when modeled within a stochastic dynamic expansion framework, alter the optimal technology mix and reduce system costs. And Ref. [19] further shows that incorporating heterogeneous demand-side resources in transmission and generation planning reduces both capital expenditure and operating costs compared with a generation-only expansion. Beyond centralized planning, demand-side flexibility is increasingly coordinated through market-based and multi-agent frameworks. In deregulated settings, a bi-level market-based investment model further shows that flexible demand reshapes generation investment decisions through both energy shifting and reserve provision [20]. A bi-level multi-energy scheduling model has been developed for virtual power plants operating in a competitive market environment [21], and a multi-objective bi-level framework has been proposed to represent the distribution system operator's behavior across the wholesale and local transactive markets [22].

DSM is particularly relevant in developing countries, where supply–demand imbalances are common and the infrastructure required for price-based demand response is often absent. While the technical potential is large, implementation of DR in developing economies is constrained by weak regulatory frameworks and limited metering infrastructure [23]. This study also identifies industrial load shifting as the most immediately practical DSM mechanism. Following this observation, our paper models two forms of industrial DSM, i.e., scheduled maintenance curtailment and flexible work-shift rescheduling. Moreover, electric vehicle adoption introduces an increasing and structurally new source of electricity demand in recent years. Load growth from EVs poses challenges to the already strained system and would require new generation capacity [24]. Nevertheless, the charging demand of EVs is flexible and could mitigate generation reliability issues if managed properly, making joint planning of generation capacity and EV flexibility with industrial demand response a practical need.

1.2.4. Decomposition algorithms for capacity expansion

The computational burden of large-scale stochastic CEP problems has motivated a range of decomposition strategies, such as Benders-based methods, Lagrangian relaxation schemes, etc [13].

Benders decomposition remains the most widely adopted framework, with recent variants addressing reliability-constrained stochastic CEP with EENS and CVaR constraints [25] and improving computational performance through regularization [26]. Lagrangian relaxation has been applied to CEP with explicit EENS constraints by dualizing the cross-scenario reliability coupling and solving the resulting subproblems via subgradient methods [27]. However, Benders-based approaches require continuous recourse for generating valid dual cuts, which is incompatible with the binary DSM scheduling variables present in the second stage of our model, and Lagrangian relaxation of cross-scenario constraints requires problem-specific feasibility recovery procedures.

The Progressive Hedging (PH) algorithm offers a scenario decomposition alternative that naturally accommodates this structure. Originally proposed for convex stochastic programs [28], PH was extended to mixed-integer problems through augmented Lagrangian relaxation of the non-anticipativity constraint [29]. Applications to stochastic energy management [30], generation and transmission planning [31], and joint battery sizing and dispatch [17] have demonstrated its suitability for problems with binary variables, while parallel implementations confirm its scalability to hundreds of scenarios [32]. PH is particularly appropriate for the present model because it decomposes the problem into independent per-scenario MILPs each containing the binary maintenance and work-shift scheduling constraints that can be solved directly by off-the-shelf solvers, while the consensus and dual update steps enforce agreement on first-stage investment decisions without requiring continuous relaxations of the integer subproblems.

1.3. Contributions and paper organization

Despite these advances, we have not found existing work that jointly integrates generation investment, decoupled BESS sizing with separate power-converter and energy-capacity decisions, flexible EV charging, and binary industrial DSM scheduling covering both maintenance and work-shift consumers within a unified risk-aware two-stage stochastic capacity expansion planning framework. To address the current research gaps, we aim to make the following contributions.

- From a modeling perspective, we propose a two-stage mixed-integer stochastic optimization model for capacity expansion planning that jointly optimizes generation investment, BESS power and energy capacities, EV charging, and industrial curtailment under demand and EV uncertainties, with system reliability handled through a Conditional Value-at-Risk (CVaR) measure on the energy not served (ENS).
- We apply the Augmented Progressive Hedging Algorithm to solve the proposed model by decomposing it into subproblems per scenario, solving each independently and analyzing its convergence behavior for the given stochastic formulation.
- For the case studies based on the Pakistani power system, we create the required input data using a multi-step reconstruction process, and the results demonstrate the value and promise of our model and solution technique.

The remainder of this paper is organized as follows. Section 2 presents the mathematical formulation of the proposed stochastic capacity expansion planning model. Section 3 describes the Progressive Hedging solution methodology. Section 4 presents case studies based on the Pakistani power system. Finally, Section 5 concludes the paper and outlines directions for future research.

2. Model

2.1. Model framework

This section presents a two-stage stochastic optimization model that co-optimizes generation investment, battery energy storage systems, electric vehicle charging, and industrial demand-side management under uncertainty. The model is formulated as a mixed-integer linear program (MILP). First-stage decisions cover new generation capacity and decoupled BESS power and energy capacities, while second-stage decisions cover generation dispatch, BESS operation, EV charging, industrial maintenance and work-shift scheduling, and load shedding. System reliability is managed by limiting the Conditional Value-at-Risk (CVaR) of the energy not served (ENS), following the Rockafellar–Uryasev formulation [33].

The model framework is shown in Fig. 1. In the subsequent sections, we present the mathematical model along with the notations, which are also collected in Appendix.

2.2. Objective function

$$
\begin{aligned}
\min \quad & \sum_{g\in\mathcal{G}} (\mathrm{IC}_g + \mathrm{FOM}_g)\, x_g + \sum_{j\in\mathcal{J}} \left(\mathrm{IC}^{\mathrm{PCS}}_j\, x^{\mathrm{PCS}}_j + \mathrm{IC}^{\mathrm{BA}}_j\, x^{\mathrm{BA}}_j \right) \\
& + \sum_{j\in\mathcal{J}} \left(\mathrm{FOM}^{\mathrm{PCS}}_j\, x^{\mathrm{PCS}}_j + \mathrm{FOM}^{\mathrm{BA}}_j\, x^{\mathrm{BA}}_j \right) \\
& + \sum_{\omega\in\Omega} P_\omega \Bigg[\sum_{t\in\mathcal{T}} \sum_{g\in\mathcal{G}} (\mathrm{MC}_g + \mathrm{VOM}_g)\, p_{g,t,\omega} \\
& \quad + \sum_{t\in\mathcal{T}} \sum_{j\in\mathcal{J}} (\mathrm{DG}_j + \mathrm{VOM}^{\mathrm{BESS}}_j)\, p^{\mathrm{dis}}_{j,t,\omega} \\
& \quad + \sum_{t\in\mathcal{T}} \sum_{n\in\mathcal{N}^{MS}} C_t\, \mu_{n,t,\omega}\, P_n \Bigg] + C^{\mathrm{sh}} \left(l^{\mathrm{VaR}} + \frac{1}{1-\alpha} \sum_{\omega\in\Omega} P_\omega\, l^{\mathrm{sh+}}_\omega \right)
\end{aligned} \tag{1a}
$$

The model minimizes the total expected cost of expanding and operating the system, augmented with a risk term, as described by (1a). The objective includes annualized capital investment costs for new generation capacity x_g across technologies g, and decoupled BESS capacities including power conversion system x^{PCS}_j with capital cost $\mathrm{IC}^{\mathrm{PCS}}_j$, and battery energy capacity x^{BA}_j with capital cost $\mathrm{IC}^{\mathrm{BA}}_j$, for each storage unit j. Fixed operation and maintenance costs FOM_g, $\mathrm{FOM}^{\mathrm{PCS}}_j$, and $\mathrm{FOM}^{\mathrm{BA}}_j$ apply annually to generation units and BESS components, respectively. Expected operational costs, weighted by scenario probability P_ω, include the variable fuel cost MC_g, variable O&M cost VOM_g for generation dispatch $p_{g,t,\omega}$; variable O&M cost $\mathrm{VOM}^{\mathrm{BESS}}_j$ and degradation cost DG_j for BESS discharge $p^{\mathrm{dis}}_{j,t,\omega}$; and the DSM cost C_t for curtailed industrial load $\mu_{n,t,\omega} P_n$, where P_n is the rated consumption of consumer n. The final term manages system reliability through the Conditional Value-at-Risk (CVaR) of load shedding at confidence level $\alpha \in [0, 1)$, weighted by a shedding-risk coefficient $C^{\mathrm{sh}} \geq 0$. The variable l^{VaR} represents the Value-at-Risk level, i.e., the total load shedding below which a fraction α of scenarios fall. The excess shedding variables $l^{\mathrm{sh+}}_\omega$ capture the amount by which total load shedding in scenario ω exceeds this level, as defined later in Section 2.3.1. The coefficient $\frac{1}{1-\alpha}$ concentrates the penalty on the worst $(1-\alpha)$ fraction of scenarios.

Setting $C^{\mathrm{sh}} = \mathrm{VOLL}$ and $\alpha = 0$ recovers the risk-neutral model.

2.3. Constraints

2.3.1. Power balance and reliability

Power balance is enforced by constraint (2a) at each time period t and scenario ω, requiring that total supply from generation, BESS discharge, DSM curtailment, and load shedding equals total demand comprising system load $D_{t,\omega}$, flexible EV charging $p^{\mathrm{EV}}_{t,\omega}$, and BESS charging. Load shedding $l^{\mathrm{sh}}_{t,\omega}$ represents unmet demand at time t under scenario ω.

$$
\sum_{g\in\mathcal{G}} p_{g,t,\omega} + \sum_{j\in\mathcal{J}} p^{\mathrm{dis}}_{j,t,\omega} + \sum_{n\in\mathcal{N}^{MS}} \mu_{n,t,\omega}\, P_n + l^{\mathrm{sh}}_{t,\omega} = D_{t,\omega} + p^{\mathrm{EV}}_{t,\omega} + \sum_{j\in\mathcal{J}} p^{\mathrm{ch}}_{j,t,\omega}, \quad \forall t\in\mathcal{T},\ \forall \omega\in\Omega. \tag{2a}
$$

Generation reliability is managed by limiting the Conditional Value-at-Risk (CVaR) of load shedding. Constraint (3a) requires the excess shedding variable $l^{\mathrm{sh+}}_\omega$ to be at least the amount by which the total scenario load shedding $\sum_{t\in\mathcal{T}} l^{\mathrm{sh}}_{t,\omega}$ exceeds the Value-at-Risk l^{VaR}. Constraints (3b) and (3c) enforce non-negativity of the excess shedding variable $l^{\mathrm{sh+}}_\omega$ and the Value-at-Risk variable l^{VaR}, respectively.

$$
l^{\mathrm{sh+}}_\omega \geq \sum_{t\in\mathcal{T}} l^{\mathrm{sh}}_{t,\omega} - l^{\mathrm{VaR}}, \quad \forall \omega\in\Omega, \tag{3a}
$$

$$
l^{\mathrm{sh+}}_\omega \geq 0, \quad \forall \omega\in\Omega, \tag{3b}
$$

$$
l^{\mathrm{VaR}} \geq 0. \tag{3c}
$$

2.3.2. Flexible demand

The flexible demand considered in this paper includes industrial DSM and smart charging for EVs. The former is explicitly modeled for two classes of flexible industrial consumers. Maintenance-based consumers $n \in \mathcal{N}^M$ are required to undergo a single annual shutdown with a predefined duration of D^M_n days. The binary variable $\mu_{n,t,\omega}$ indicates whether consumer n is curtailed at time t in scenario ω. Constraint (4a) enforces the total curtailment duration over the entire horizon. Contiguity of the maintenance period is ensured through the start indicator $\upsilon_{n,t,\omega}$ using constraint (4b). The curtailment status is tracked over time using the state-transition constraint (4d). Constraints (4e) and (4f) guarantee a unique start and end of the maintenance event, and constraint (4g) restricts maintenance initiation to daily boundaries.

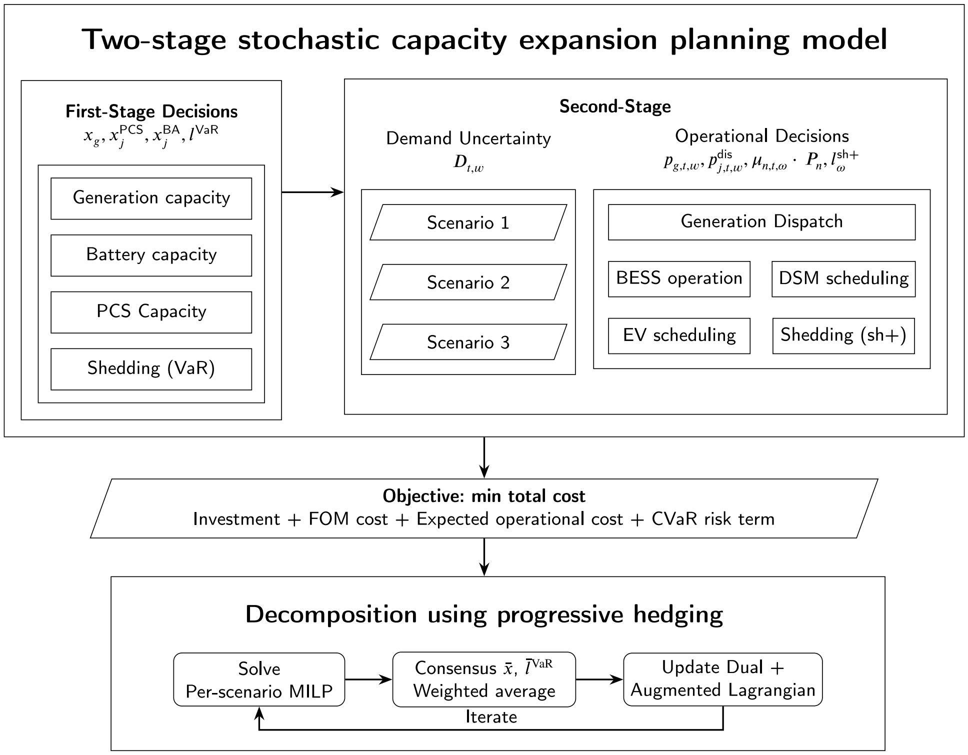

Fig. 1. Representation of the proposed scheme, which consists of the two-stage stochastic capacity expansion planning model and the Progressive Hedging decomposition. The upper panel illustrates the two-stage stochastic model: the first stage determines generation and storage investment decisions while the second stage optimizes dispatch with flexible demand across demand scenarios. The lower panel depicts the Progressive Hedging algorithm, which decomposes the full problem into independent per-scenario MILPs. System reliability is managed through a Conditional Value-at-Risk (CVaR) formulation.

$$\sum_{t\in\mathcal{T}} \mu_{n,t,\omega} = 24 \cdot D_n^{\mathrm{M}}, \quad \forall n \in \mathcal{N}^{\mathrm{M}},\ \forall \omega \in \Omega, \tag{4a}$$

$$\sum_{t'=t-24\cdot D_n^{\mathrm{M}}+1}^{t} v_{n,t',\omega} \le \mu_{n,t,\omega}, \quad \forall n \in \mathcal{N}^{\mathrm{M}},\ \forall t \ge 24 \cdot D_n^{\mathrm{M}},\ \forall \omega \in \Omega, \tag{4b}$$

$$\mu_{n,t,\omega} \le v_{n,t,\omega}, \quad \forall n \in \mathcal{N}^{\mathrm{M}},\ t = 1,\ \forall \omega \in \Omega, \tag{4c}$$

$$\mu_{n,t,\omega} = \mu_{n,t-1,\omega} + v_{n,t,\omega} - z_{n,t,\omega}, \quad \forall n \in \mathcal{N}^{\mathrm{M}},\ \forall t \in \mathcal{T} \setminus \{1\},\ \forall \omega \in \Omega, \tag{4d}$$

$$\sum_{t\in\mathcal{T}} v_{n,t,\omega} = 1, \quad \forall n \in \mathcal{N}^{\mathrm{M}},\ \forall \omega \in \Omega, \tag{4e}$$

$$\sum_{t\in\mathcal{T}} z_{n,t,\omega} = 1, \quad \forall n \in \mathcal{N}^{\mathrm{M}},\ \forall \omega \in \Omega, \tag{4f}$$

$$v_{n,t,\omega} = 0, \quad \text{if } (t-1) \bmod 24 \ne 0,\ \forall n \in \mathcal{N}^{\mathrm{M}},\ \forall \omega \in \Omega, \tag{4g}$$

Work-shift consumers $n \in \mathcal{N}^{\mathrm{S}}$ are modeled with flexible weekly operation schedules. For each week $w \in \mathcal{W}$, the total curtailment duration is enforced by (5a) using the required number of curtailed days D_n^{S}. Contiguity of shift curtailment is imposed through (5b), while the evolution of the curtailment state is governed by (5d), with the same boundary treatment at the first period as in the industry case. Constraints (5e) and (5f) ensure exactly one start and one end event per week, and constraint (5g) aligns all scheduling decisions with daily boundaries.

Note that the model does not introduce additional curtailment on top of the maintenance and work-shift patterns. Rather, it co-optimizes the timing of these pre-existing off-periods within the capacity expansion plan, shifting them toward hours of system stress.

$$\sum_{t\in\mathcal{T}_w} \mu_{n,t,\omega} = 24\, D_n^{\mathrm{S}}, \quad \forall n \in \mathcal{N}^{\mathrm{S}},\ \forall w \in \mathcal{W},\ \forall \omega \in \Omega, \tag{5a}$$

$$\sum_{t'=t-24D_n^{\mathrm{S}}+1}^{t} v_{n,t',\omega} \le \mu_{n,t,\omega}, \quad \forall n \in \mathcal{N}^{\mathrm{S}},\ \forall t \ge 24D_n^{\mathrm{S}},\ \forall \omega \in \Omega, \tag{5b}$$

$$\mu_{n,t,\omega} \le v_{n,t,\omega}, \quad \forall n \in \mathcal{N}^{\mathrm{S}},\ t = 1,\ \forall \omega \in \Omega, \tag{5c}$$

$$\mu_{n,t,\omega} = \mu_{n,t-1,\omega} + v_{n,t,\omega} - z_{n,t,\omega}, \quad \forall n \in \mathcal{N}^{\mathrm{S}},\ \forall t \in \mathcal{T} \setminus \{1\},\ \forall \omega \in \Omega, \tag{5d}$$

$$\sum_{t\in\mathcal{T}_w} v_{n,t,\omega} = 1, \quad \forall n \in \mathcal{N}^{\mathrm{S}},\ \forall w \in \mathcal{W},\ \forall \omega \in \Omega, \tag{5e}$$

$$\sum_{t\in\mathcal{T}_w} z_{n,t,\omega} = 1, \quad \forall n \in \mathcal{N}^{\mathrm{S}},\ \forall w \in \mathcal{W},\ \forall \omega \in \Omega, \tag{5f}$$

$$v_{n,t,\omega} = 0, \quad \text{if } (t-1) \bmod 24 \ne 0,\ \forall n \in \mathcal{N}^{\mathrm{S}},\ \forall \omega \in \Omega. \tag{5g}$$

Electric vehicle charging is modeled as a flexible load that can be scheduled optimally within availability windows. The maximum charging power for scenario ω is computed as $P_\omega^{\mathrm{EV}} = \frac{\phi_\omega}{100} \cdot \max_{t\in\mathcal{T}}\{D_t \cdot \lambda_\omega\}$, where ϕ_ω is the scenario-specific EV penetration fraction and λ_ω is the demand scaling factor. Constraint (6a) bounds charging at each period by this maximum power scaled by availability factor $\alpha_{h(t)}^{\mathrm{EV}} \in [0,1]$, which represents the fraction of EVs connected to the grid at hour-of-day $h(t) = ((t-1) \bmod 24) + 1$. Constraint (6b) ensures that each day $d \in \mathcal{D}$ receives the required total energy, computed as the product of maximum charging power, 24 h, and average daily availability $\bar{\alpha}^{\mathrm{EV}} = \frac{1}{24}\sum_{h=1}^{24} \alpha_h^{\mathrm{EV}}$, where $\mathcal{H}_d$ denotes the set of 24 h in day d.

$$p_{t,\omega}^{\mathrm{EV}} \le \alpha_{h(t)}^{\mathrm{EV}} \cdot P_\omega^{\mathrm{EV}}, \quad \forall t \in \mathcal{T},\ \forall \omega \in \Omega, \tag{6a}$$

$$\sum_{t\in\mathcal{H}_d} p_{t,\omega}^{\mathrm{EV}} = 24 \cdot \bar{\alpha}^{\mathrm{EV}} \cdot P_\omega^{\mathrm{EV}}, \quad \forall d \in \mathcal{D},\ \forall \omega \in \Omega. \tag{6b}$$

2.3.3. Generation and storage limits

$$p_{g,t,\omega} \le (\tilde{x}_g + x_g)\, \rho_{g,t} \quad \forall g \in \mathcal{G},\ \forall t \in \mathcal{T},\ \forall \omega \in \Omega. \tag{7a}$$

$$e_{j,t,\omega} = E_0 + \eta^{\mathrm{ch}}\, p^{\mathrm{ch}}_{j,t,\omega} - \frac{1}{\eta^{\mathrm{dis}}}\, p^{\mathrm{dis}}_{j,t,\omega}, \quad \forall j \in \mathcal{J},\ t = 1,\ \forall \omega \in \Omega, \tag{7b}$$

$$e_{j,t,\omega} = e_{j,t-1,\omega} + \eta^{\mathrm{ch}}\, p^{\mathrm{ch}}_{j,t,\omega} - \frac{1}{\eta^{\mathrm{dis}}}\, p^{\mathrm{dis}}_{j,t,\omega}, \quad \forall j \in \mathcal{J},\ \forall t \in \mathcal{T} \setminus \{1\},\ \forall \omega \in \Omega, \tag{7c}$$

$$p^{\mathrm{ch}}_{j,t,\omega} \le \tilde{x}^{\mathrm{PCS}}_j + x^{\mathrm{PCS}}_j, \quad \forall j \in \mathcal{J},\ \forall t \in \mathcal{T},\ \forall \omega \in \Omega, \tag{7d}$$

$$p^{\mathrm{dis}}_{j,t,\omega} \le \tilde{x}^{\mathrm{PCS}}_j + x^{\mathrm{PCS}}_j, \quad \forall j \in \mathcal{J},\ \forall t \in \mathcal{T},\ \forall \omega \in \Omega, \tag{7e}$$

$$e_{j,t,\omega} \le \tilde{x}^{\mathrm{BA}}_j + x^{\mathrm{BA}}_j, \quad \forall j \in \mathcal{J},\ \forall t \in \mathcal{T},\ \forall \omega \in \Omega, \tag{7f}$$

$$e_{j,t,\omega} = E_0, \quad \forall j \in \mathcal{J},\ \forall t \in \{24, 48, \dots, |\mathcal{T}|\},\ \forall \omega \in \Omega. \tag{7g}$$

Constraint (7a) bounds power generation by installed capacity, comprising existing capacity $\tilde{x}_g$ and new investment x_g, multiplied by availability factor $\rho_{g,t}$ which equals unity for conventional units and follows meteorological profiles for solar and wind resources. The BESS power variables $p^{\mathrm{ch}}_{j,t,\omega}$ and $p^{\mathrm{dis}}_{j,t,\omega}$ are defined at the grid terminal of the storage unit, and the BESS dynamics are governed by constraints (7b) through (7g), applied to each storage unit $j \in \mathcal{J}$. Since the first period has no predecessor, constraint (7b) initializes the state-of-charge from reference level E_0, while constraint (7c) tracks its evolution for all subsequent periods in which conversion losses are represented by multiplying the charging power $p^{\mathrm{ch}}_{j,t,\omega}$ by the charging efficiency η^{ch} and dividing the discharging power $p^{\mathrm{dis}}_{j,t,\omega}$ by the discharging efficiency η^{dis}, yielding a round-trip efficiency of $\eta^{\mathrm{ch}}\eta^{\mathrm{dis}}$. Constraints (7d) and (7e) bound charging and discharging rates by total installed PCS capacity of unit j, comprising existing capacity $\tilde{x}^{\mathrm{PCS}}_j$ and new investment x^{PCS}_j. Constraint (7f) limits state-of-charge by total battery energy capacity, comprising existing capacity $\tilde{x}^{\mathrm{BA}}_j$ and new investment x^{BA}_j. Constraint (7g) resets state-of-charge to E_0 at the end of each day, simulating a daily cycle. The case study presented in Section 4 uses a single BESS unit ($|\mathcal{J}| = 1$), but the formulation generalizes to multiple units.

3. Decomposition via progressive hedging

The proposed MILP model poses computational challenges with multiple coupled scenarios, therefore we employ the Progressive Hedging (PH) algorithm as depicted in the lower panel of Fig. 1 to solve it. In PH, a copy of each first-stage variable is created for each scenario, and the nonanticipativity constraint enforcing equality across scenarios is relaxed and dualized. In addition to the conventional Lagrangian term added to the objective, a proximal (quadratic penalty) term is included, yielding an augmented Lagrangian subproblem for each scenario $\omega \in \Omega$. In the convex case, standard strong duality guarantees convergence of the Progressive Hedging algorithm for an adequate choice of the penalty parameters. However, because of the presence of binary variables in the second-stage DSM scheduling decisions, the scenario subproblems are mixed-integer programs and the overall problem is non-convex. Consequently, neither convergence nor optimality at convergence is formally guaranteed, and the PH algorithm remains a heuristic for our non-convex problem. A more detailed description of PH itself is beyond the scope of this paper, and we refer interested readers to [29].

The PH framework decomposes the full problem into independent scenario subproblems, each a MILP solved separately using solvers, enabling straightforward parallelization across scenarios. Non-anticipativity is enforced on the first-stage investment variables (x_g, x^{PCS}_j, x^{BA}_j), which are common to all scenarios. By contrast, the binary maintenance and work-shift indicators ($\mu_{n,t,\omega}$, $v_{n,t,\omega}$, $z_{n,t,\omega}$) are second-stage recourse decisions that are realized after the demand and EV-penetration scenario is observed. Therefore, they are allowed to differ across scenarios by construction and require no consensus. This is the defining structure of the two-stage stochastic program, in which non-anticipativity applies to the first-stage decisions, and the PH consensus and dual updates act on the first-stage variables accordingly.

In addition, the CVaR risk term couples the scenarios through the scalar Value-at-Risk variable l^{VaR}, which is treated as an additional first-stage non-anticipative variable, so each scenario subproblem keeps a local copy l^{VaR}_ω, and consensus on l^{VaR} is reached through similar probability-weighted averaging and dual update, while the scenario-local excess load shedding variables $l^{\mathrm{sh}+}_\omega$ require no consensus. The risk term therefore preserves the full scenario decomposition without introducing scenario-coupling constraints. Our PH implementation is provided in Algorithm 1 and detailed below.

For each scenario ω, we solve subproblem (8).

$$\begin{aligned}\mathcal{L}_\omega = {} & \sum_{g\in\mathcal{G}} (\mathrm{IC}_g + \mathrm{FOM}_g)\, x_{g,\omega} + \sum_{j\in\mathcal{J}} \Big((\mathrm{IC}^{\mathrm{PCS}}_j + \mathrm{FOM}^{\mathrm{PCS}}_j)\, x^{\mathrm{PCS}}_{j,\omega} \\ & + (\mathrm{IC}^{\mathrm{BA}}_j + \mathrm{FOM}^{\mathrm{BA}}_j)\, x^{\mathrm{BA}}_{j,\omega} \Big) + \sum_{t\in\mathcal{T}} \sum_{g\in\mathcal{G}} (\mathrm{MC}_g + \mathrm{VOM}_g)\, p_{g,t,\omega} \\ & + \sum_{t\in\mathcal{T}} \sum_{j\in\mathcal{J}} (\mathrm{DG}_j + \mathrm{VOM}^{\mathrm{BESS}}_j)\, p^{\mathrm{dis}}_{j,t,\omega} \\ & + \sum_{t\in\mathcal{T}} \sum_{n\in\mathcal{N}^{MS}} C_t\, \mu_{n,t,\omega}\, P_n + C^{\mathrm{sh}} \left(l^{\mathrm{VaR}}_\omega + \frac{1}{1-\alpha}\, l^{\mathrm{sh}+}_\omega \right) \\ & + \sum_{g\in\mathcal{G}} \left[w_{g,\omega} (x_{g,\omega} - \bar{x}_g) + \frac{\rho_g}{2} (x_{g,\omega} - \bar{x}_g)^2 \right] \\ & + \sum_{j\in\mathcal{J}} \left[w^{\mathrm{PCS}}_{j,\omega} (x^{\mathrm{PCS}}_{j,\omega} - \bar{x}^{\mathrm{PCS}}_j) + \frac{\rho^{\mathrm{PCS}}_j}{2} (x^{\mathrm{PCS}}_{j,\omega} - \bar{x}^{\mathrm{PCS}}_j)^2 \right] \\ & + \sum_{j\in\mathcal{J}} \left[w^{\mathrm{BA}}_{j,\omega} (x^{\mathrm{BA}}_{j,\omega} - \bar{x}^{\mathrm{BA}}_j) + \frac{\rho^{\mathrm{BA}}_j}{2} (x^{\mathrm{BA}}_{j,\omega} - \bar{x}^{\mathrm{BA}}_j)^2 \right] \\ & + w^{\mathrm{VaR}}_\omega (l^{\mathrm{VaR}}_\omega - \bar{l}^{\mathrm{VaR}}) + \frac{\rho^{\mathrm{VaR}}}{2} (l^{\mathrm{VaR}}_\omega - \bar{l}^{\mathrm{VaR}})^2, \end{aligned} \tag{8}$$

s.t. (2a)–(7g)

where $\bar{x}_g$, $\bar{x}^{\mathrm{PCS}}_j$, and $\bar{x}^{\mathrm{BA}}_j$ are the current consensus targets, $w_{g,\omega}$, $w^{\mathrm{PCS}}_{j,\omega}$, and $w^{\mathrm{BA}}_{j,\omega}$ are the dual multipliers, and ρ_g, ρ^{PCS}_j, $\rho^{\mathrm{BA}}_j > 0$ are the penalty parameters. Analogously, $\bar{l}^{\mathrm{VaR}}$ is the consensus target for the Value-at-Risk variable, w^{VaR}_ω its dual multiplier, and $\rho^{\mathrm{VaR}} > 0$ its penalty parameter. All dual multipliers are initialized to zero.

After all scenario subproblems are solved at iteration k, the consensus targets and Value-at-Risk variable l^{VaR} are updated as probability-weighted averages, as in (9a)–(9d).

$$\bar{x}^{k+1}_g = \sum_{\omega\in\Omega} P_\omega\, x^k_{g,\omega}, \quad \forall g \in \mathcal{G}, \tag{9a}$$

$$\bar{x}^{\mathrm{PCS},k+1}_j = \sum_{\omega\in\Omega} P_\omega\, x^{\mathrm{PCS},k}_{j,\omega}, \quad \forall j \in \mathcal{J}, \tag{9b}$$

$$\bar{x}^{\mathrm{BA},k+1}_j = \sum_{\omega\in\Omega} P_\omega\, x^{\mathrm{BA},k}_{j,\omega}, \quad \forall j \in \mathcal{J}, \tag{9c}$$

$$\bar{l}^{\mathrm{VaR},k+1} = \sum_{\omega\in\Omega} P_\omega\, l^{\mathrm{VaR},k}_\omega. \tag{9d}$$

The dual multipliers are then updated using the deviation of each scenario solution from the consensus, as in (10a)–(10d).

$$w^{k+1}_{g,\omega} = w^k_{g,\omega} + \rho_g (x^k_{g,\omega} - \bar{x}^k_g), \quad \forall g \in \mathcal{G},\ \forall \omega \in \Omega, \tag{10a}$$

$$w^{\mathrm{PCS},k+1}_{j,\omega} = w^{\mathrm{PCS},k}_{j,\omega} + \rho^{\mathrm{PCS}}_j (x^{\mathrm{PCS},k}_{j,\omega} - \bar{x}^{\mathrm{PCS},k}_j), \quad \forall j \in \mathcal{J},\ \forall \omega \in \Omega, \tag{10b}$$

$$w^{\mathrm{BA},k+1}_{j,\omega} = w^{\mathrm{BA},k}_{j,\omega} + \rho^{\mathrm{BA}}_j (x^{\mathrm{BA},k}_{j,\omega} - \bar{x}^{\mathrm{BA},k}_j), \quad \forall j \in \mathcal{J},\ \forall \omega \in \Omega, \tag{10c}$$

$$w^{\mathrm{VaR},k+1}_\omega = w^{\mathrm{VaR},k}_\omega + \rho^{\mathrm{VaR}} (l^{\mathrm{VaR},k}_\omega - \bar{l}^{\mathrm{VaR},k}), \quad \forall \omega \in \Omega. \tag{10d}$$

Penalty parameters are initialized using a cost-proportional strategy so that penalty magnitudes are commensurate with the scale of each investment decision, as in (11a)–(11c). The penalty for the Value-at-Risk variable is scaled by the risk weight, as in (11d).

$$\rho^{(0)}_g = \rho_{\mathrm{base}} \cdot (\mathrm{IC}_g + \mathrm{FOM}_g), \quad \forall g \in \mathcal{G}, \tag{11a}$$

$$\rho^{\mathrm{PCS},(0)}_j = \rho_{\mathrm{base}} \cdot (\mathrm{IC}^{\mathrm{PCS}}_j + \mathrm{FOM}^{\mathrm{PCS}}_j), \quad \forall j \in \mathcal{J}, \tag{11b}$$

$$\rho^{\mathrm{BA},(0)}_j = \rho_{\mathrm{base}} \cdot (\mathrm{IC}^{\mathrm{BA}}_j + \mathrm{FOM}^{\mathrm{BA}}_j), \quad \forall j \in \mathcal{J}, \tag{11c}$$

Algorithm 1 Progressive Hedging Algorithm

Input: Scenarios Ω with probabilities $\{P_\omega\}$, cost data, tolerances $\epsilon_{\mathrm{abs}}, \epsilon_{\mathrm{rel}}, \epsilon_{\mathrm{obj}}, \epsilon_{\mathrm{dev}}$, max iterations $K_{\max}$.
Output: Consensus capacities $\bar{x}_g, \bar{x}^{\mathrm{PCS}}, \bar{x}^{\mathrm{BA}}$ and VaR $\bar{l}^{\mathrm{VaR}}$.
// Phase 1: Initialization
for each $\omega \in \Omega$ **do**
  Solve the *unaugmented* subproblem (8) ($w = 0,\ \rho = 0,\ \bar{x} = 0,\ \bar{l}^{\mathrm{VaR}} = 0$).
  Record $x^0_{g,\omega}, x^{\mathrm{PCS},0}_\omega, x^{\mathrm{BA},0}_\omega, l^{\mathrm{VaR},0}_\omega$.
end for
Initialize all dual multipliers to 0.
Set $\rho_g, \rho^{\mathrm{PCS}}, \rho^{\mathrm{BA}}, \rho^{\mathrm{VaR}}$ via Eqs. (11a)–(11d).
Compute initial consensus via Eqs. (9a)–(9d).
// Phase 2: PH iterations
for $k = 1, 2, \ldots, K_{\max}$ **do**
  Update consensus $\bar{x}^k, \bar{l}^{\mathrm{VaR},k}$ via Eqs. (9a)–(9d).
  for each $\omega \in \Omega$ **do**
    Solve augmented subproblem (8) using the current consensus $\bar{x}^k, \bar{l}^{\mathrm{VaR},k}$ and multipliers w_ω.
    Record $x^k_{g,\omega}, x^{\mathrm{PCS},k}_\omega, x^{\mathrm{BA},k}_\omega, l^{\mathrm{VaR},k}_\omega$.
  end for
  Update dual multipliers via Eqs. (10a)–(10d).
  Compute r^k (12a), r^k_{rel} (12b), $\mathbb{E}[f^k]$, and the maximum deviation as in (13).
  if all four criteria in (13) are satisfied **then**
    break
  end if
end for
Return $\bar{x}^k_g, \bar{x}^{\mathrm{PCS},k}, \bar{x}^{\mathrm{BA},k}, \bar{l}^{\mathrm{VaR},k}$.

$$\rho^{\mathrm{VaR},(0)} = \rho_{\mathrm{base}} \cdot C^{\mathrm{sh}}. \tag{11d}$$

The algorithm evaluates convergence using four complementary metrics, computed over the first-stage capacity variables and the Value-at-Risk variable l^{VaR}. The primal residual quantifies the probability-weighted deviation of scenario-specific decisions from the consensus solution, as defined in (12a), while the relative primal residual provides a scale-independent measure by normalizing this value with the Euclidean norm of the consensus vector, as given in (12b).

$$r^k = \Bigg[\sum_{\omega\in\Omega} P_\omega\Big(\sum_{g\in\mathcal{G}}\big(x^k_{g,\omega} - \bar{x}^k_g\big)^2 + \sum_{j\in\mathcal{J}}\big(x^{\mathrm{PCS},k}_{j,\omega} - \bar{x}^{\mathrm{PCS},k}_j\big)^2 + \sum_{j\in\mathcal{J}}\big(x^{\mathrm{BA},k}_{j,\omega} - \bar{x}^{\mathrm{BA},k}_j\big)^2 + \big(l^{\mathrm{VaR},k}_\omega - \bar{l}^{\mathrm{VaR},k}\big)^2\Big)\Bigg]^{1/2}, \tag{12a}$$

$$r^k_{\mathrm{rel}} = \frac{r^k}{\Big[\sum_{g\in\mathcal{G}}\big(\bar{x}^k_g\big)^2 + \sum_{j\in\mathcal{J}}\big(\bar{x}^{\mathrm{PCS},k}_j\big)^2 + \sum_{j\in\mathcal{J}}\big(\bar{x}^{\mathrm{BA},k}_j\big)^2 + \big(\bar{l}^{\mathrm{VaR},k}\big)^2\Big]^{1/2}} \times 100\%. \tag{12b}$$

Convergence is achieved when all four of the following conditions are simultaneously satisfied.

$$r^k < \epsilon_{\mathrm{abs}},\quad r^k_{\mathrm{rel}} < \epsilon_{\mathrm{rel}},\quad \left|\frac{\mathbb{E}[f^k] - \mathbb{E}[f^{k-1}]}{\mathbb{E}[f^{k-1}]}\right| < \epsilon_{\mathrm{obj}},$$
$$\max\Big\{\max_{\omega,g}\big|x^k_{g,\omega} - \bar{x}^k_g\big|,\ \max_{\omega,j}\big|x^{\mathrm{PCS},k}_{j,\omega} - \bar{x}^{\mathrm{PCS},k}_j\big|,\ \max_{\omega,j}\big|x^{\mathrm{BA},k}_{j,\omega} - \bar{x}^{\mathrm{BA},k}_j\big|,\ \max_{\omega}\big|l^{\mathrm{VaR},k}_\omega - \bar{l}^{\mathrm{VaR},k}\big|\Big\} < \epsilon_{\mathrm{dev}}. \tag{13}$$

Here, $\mathbb{E}[f^k] = \sum_{\omega\in\Omega} P_\omega f^k_\omega$ denotes the probability-weighted expected objective value.

4. Case studies

In this section, we explain and discuss a set of numerical tests that demonstrate the value of the proposed approach using Pakistan's power system, and the analysis is conducted in a forward-looking setting of year 2030, to capture both medium-term investment decisions and short-term operational variations.

4.1. Data construction and assumptions

4.1.1. Generation technologies and BESS

Legacy and candidate generation technologies are derived from the Indicative Generation Capacity Expansion Plan (IGCEP) published by the National Transmission and Dispatch Company (NTDC) [34]. The generation portfolio includes lignite, coal, biomass, open-cycle gas turbines (OCGT), combined-cycle gas turbines (CCGT), wind, solar photovoltaic (PV), and utility-scale BESS. Tables 1 and 2 present the economic parameters of generation technologies and BESS. Fuel costs and both variable and fixed operation and maintenance (O&M) costs are based on the latest tariff determinations and quarterly indexation reports published by the National Electric Power Regulatory Authority (NEPRA) [35]. BESS parameters are adopted from the IGCEP report [36]. Other parameters, including forecasted investment costs and emission factors, are sourced from [37,38], as these are not publicly available for Pakistan.

To model renewable generation in the capacity expansion framework, hourly capacity factor profiles are developed for both wind and solar technologies. Wind resource characterization is conducted using measured daily production data from operational wind farms in Pakistan for 2016, obtained from NTDC [34]. The daily generation profile was downscaled to hourly resolution using NASA MERRA-2 reanalysis wind speed data [39] for the same geographic coordinates and time period. The downscaling methodology employed a cubic power-wind speed relationship, distributing hourly generation proportionally to the cube of hourly wind speeds while preserving daily energy totals. The resulting hourly profile was normalized and scaled to achieve a target annual capacity factor of 42% for 2030 projections, reflecting anticipated improvements in turbine technology and optimal site selection [40].

In the absence of operational solar generation data from NTDC, solar capacity factor profiles were synthesized using NASA CERES SYN1deg satellite-derived irradiance data [39] for 2024. A composite hourly profile was constructed by combining Global Horizontal Irradiance (GHI) measurements from three major solar installations (Bahawalpur, Layyah, and Sukkur), weighted by their respective installed capacities. Hourly capacity factors were computed as $\mathrm{CF}_h = (\mathrm{GHI}_h/1000) \times \mathrm{PR}$, where PR denotes the performance ratio, set at 0.80 to account for temperature derating, soiling losses, inverter efficiency, and other system losses [41]. The composite profile was normalized and scaled to a target annual capacity factor of 23% for 2030, consistent with projected solar technology improvements.

4.1.2. System load

The system load profile is characterized on an hourly basis across the planning horizon, encompassing three peak demand growth scenarios developed by NTDC [36], as depicted in Fig. 2(a). The long-term electricity peak demand forecast distinguishes between low, normal, and high growth trajectories to account for uncertainty in macroeconomic conditions and sectoral development patterns. The normal growth scenario is adopted to construct the hourly demand profile for 2030.

Since hourly load data is not directly available from NTDC, the methodology employs a multi-step reconstruction process. First, a baseline hourly load profile for 2016 is constructed by combining daily peak demand data and a representative daily load curve, both of which are

Table 1
Economic parameters of candidate generation technologies.

Technology	Existing capacity (MW)	Investment cost (€/MW/yr)	Fixed O&M (€/MW/yr)	Variable O&M (€/MWh)	Fuel cost (€/MWh)	Emission factor (tCO_2/MWh)
Lignite	3960	127,714	32,500	4.5	82.43	1.10
Coal	3300	113,523	25,600	3.6	91.34	0.95
CCGT	4046	54,633	15,000	2.0	78.49	0.40
Biomass	364	127,714	40,100	3.56	100.22	0.10
OCGT	6492	49,666	15,000	11.0	107.79	0.60
Wind	1845	82,375	14,000	0.18	0.00	0.00
Solar PV	650	47,041	10,800	0.0	0.00	0.00

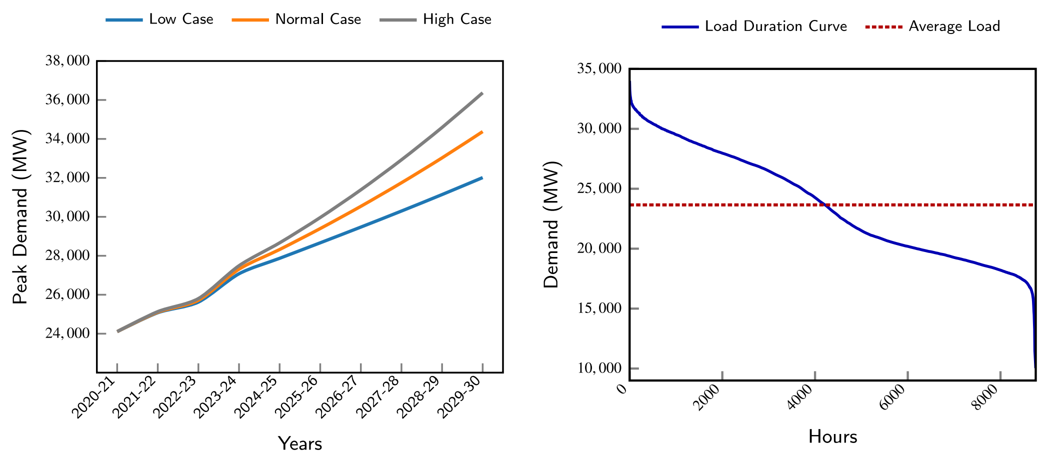

(a) Forecasted Peak Demand (2020-2030)

(b) Load Duration Curve for 2030

Fig. 2. Peak demand forecast and load characteristics of the Pakistani power system: (a) forecasted peak demand from 2020 to 2030 by NTDC, and (b) load duration curve for 2030 created in this study.

Table 2
Economic and operational parameters of battery energy storage system.

Parameter	PCS	Battery
Existing capacity	50 MW	100 MWh
Investment cost	10,296 €/MW/yr	20,592 €/MWh
Fixed O&M cost	3000 €/MW/yr	8000 €/MWh/yr
Variable O&M cost	0.001 €/MWh	0.001 €/MWh
Charging efficiency	95%	
Discharging efficiency	95%	
Degradation cost	5.0 €/MWh	

publicly available on the NTDC website [34]. This reconstructed baseline preserves the typical diurnal, weekly, and seasonal load variations characteristic of the Pakistani power system. The profile is normalized by the 2016 peak demand and scaled to the forecasted 2030 peak demand under the normal case, yielding a scaling factor of 1.4656. This proportional scaling preserves temporal load characteristics while reflecting anticipated system growth, resulting in a profile of year 2030 with an average demand of 23,653 MW and a system load factor of 69.57%. The corresponding load duration curve, presented in Fig. 2(b), exhibits a peak-to-minimum ratio of 3.39. For the case studies presented in this work, this profile is further scaled to derive three scenarios representing 80%, 100%, and 120% of the baseline demand projection, assigned probabilities of 0.25, 0.50, and 0.25 in line with the demand scenarios, yielding 3×8760 hourly time steps for analysis.

System reliability is managed through the Conditional Value-at-Risk (CVaR) of load shedding computed at a confidence level $\alpha = 0.95$, which captures the expected load shedding across the worst $(1-\alpha)$ fraction of scenarios. The model prices load shedding exclusively through the CVaR risk term, weighted by a shedding-risk coefficient C^{sh} and the value of it assumed to be €10,000/MWh.

4.1.3. Flexible demand

Electric vehicle integration is modeled to evaluate the power system's capability to accommodate projected charging demand. Across the demand scenarios, EV fleet penetration levels of 5%, 6%, and 7% are examined to assess system impacts under the progressive electrification of the transportation sector. Baseline EV charging load is assumed to constitute approximately 0.05% of current peak demand. Due to the early stage of EV adoption in Pakistan and the lack of comprehensive data on charging infrastructure capacity, EV demand is modeled as an additional load proportional to the system peak demand. Charging behavior is characterized using time-varying availability factors derived from empirical data collected at a 630 kVA public charging station, capturing representative daily charging patterns with peak demand occurring during evening hours. The normalized charging availability profile is illustrated in Fig. 3. We also conduct a sensitivity analysis on the shape of charging availability profile in Section 4.2.3

Industrial demand-side management is modeled as two types of flexible consumers, including maintenance-based consumers with annual shutdown requirements and work-shift consumers with adjustable weekly operating schedules. According to the IGCEP annual report in 2021, industrial consumption in Pakistan accounts for 23% of total electricity demand [36]. Furthermore, based on the energy demand forecasting analysis conducted for Pakistan using the LEAP model, in 2030 the demand response potential is estimated to be 3.8% of the peak load [42]. In this study, the total number of consumers considered for curtailment is assumed to represent 15% of all current industrial consumers. The operational characteristics of these flexible loads, including flexibility constraints, penalty costs, and the number of maintenance or off days associated with load shifting, are adopted from [43]. The curtailment cost for these consumers is assumed to be twice the fuel cost of the most expensive candidate generation technology, and remains uniform across all working days of the week

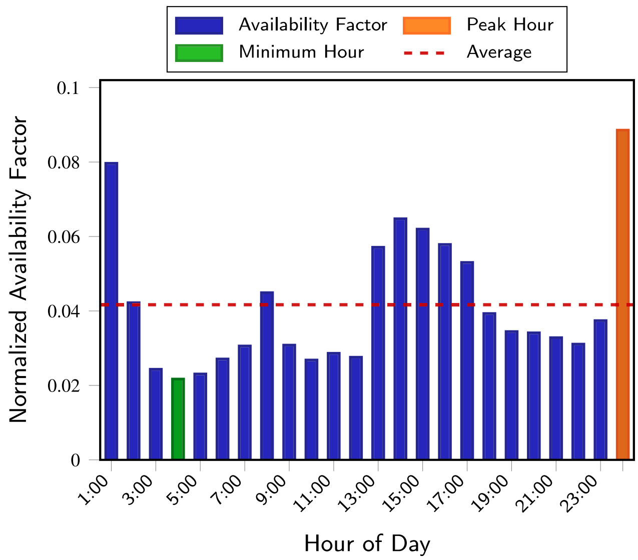

Fig. 3. Normalized hourly EV charging availability profile.

Table 3
Parameters of maintenance consumers.

Maintenance ID	Maintenance power [MW]	Maintenance duration [Day]
M1	100	3
M2	90	4
M3	80	3
M4	70	7
M5	60	3
M6	100	3
M7	100	3
M8	90	3
M9	90	3

Table 4
Parameters of work-shift consumers.

Work-shift ID	Work-shift power [MW]	Work-shift duration [Day]
S1	60	2
S2	60	2
S3	70	2
S4	80	2
S5	100	2
S6	110	2
S7	120	2
S8	130	2
S9	140	2

and zero for Saturdays and Sundays treated as off days. The corresponding parameters for maintenance-based and shift-based consumers are summarized in Tables 3 and 4.

4.2. Results and discussion

To quantify the contribution of each flexibility source, three cases are analyzed. In Case 1, industrial demand is assumed to be fully inelastic and EV charging is incorporated without smart-charging capability, representing a scenario in which EV load adds to system demand without offering any scheduling flexibility. In Case 2, the full framework co-optimizes maintenance scheduling, weekly work-shift adjustments, and flexible EV charging. In Case 3, demand-side flexibility is limited to industrial maintenance and work-shift scheduling, while EV charging is included without smart-charging capability. In the following, we first evaluate the performance of the Progressive Hedging decomposition in Section 4.2.1. Then Section 4.2.2 compares the results of the proposed model against the deterministic approach using Case 2. Based on the proposed model, Section 4.2.3 analyzes and compares the investment and operational outcomes across all three cases. Section 4.2.4 assesses the impact of CVaR on system cost and load shedding.

Table 5
Model statistics in different cases and performance of the decomposition approach.

Metric	Case 1	Case 2	Case 3
Model statistics			
Continuous variables	289,140	788,460	762,180
Binary variables	0	1,419,120	1,419,120
Constraints	342,765	2,246,883	2,215,620
Performance of PH			
Iterations	–	31	30
Primal residual (MW)	–	0.4	0.4
Relative residual (%)	–	0.001	0.001
Objective change (%)	–	0.001	0.001
Max capacity deviation (MW/MWh)	–	1.07	1.09

4.2.1. Performance of the decomposition approach

Table 5 summarizes the model dimensions and convergence performance across the three cases. The algorithm is considered converged when four predefined criteria are met simultaneously, i.e., primal residual below $\epsilon_{\text{abs}} = 1.0\,\text{MW}$, relative residual below $\epsilon_{\text{rel}} = 0.2\%$, objective change less than 0.2% between successive iterations, and maximum first-stage deviation across scenarios within 2.0 MW. To reduce computational overhead, each subproblem is built only once during the initialization phase. In all subsequent PH iterations, only the consensus targets $\bar{x}$, dual multipliers w, and penalty weights ρ are updated, while the model structure itself is preserved. The penalty parameters are initialized in proportion to each technology's investment cost as in Eqs. (11a)–(11c) using a single base scaling factor $\rho_{\text{base}} = 0.005$, held constant across all iterations, which keeps the augmented Lagrangian terms well scaled across technologies with different capital costs.

Among the three cases, Case 2 is the most computationally demanding due to the binary work-shift scheduling variables in the DSM formulation and the flexible charging of EVs, yielding the largest model dimensions. The final primal residuals of Case 2 and 3 are well within the prescribed tolerances, as shown in the lower section of Table 5, confirming that the decomposition approach produces consistent, consensus-based investment decisions while remaining tractable for a large-scale MILP with combinatorial DSM constraints.

4.2.2. Performance of the two-stage stochastic programming model

To evaluate the advantages of accounting for uncertainty in capacity expansion decisions, the proposed two-stage stochastic model solved via Progressive Hedging is compared against a Deterministic Formulation (DF). In the DF, all uncertain parameters are replaced by their probability-weighted average. This benchmark corresponds to the expected result of using the expected value solution (EEV), in which the mean-value problem is solved and its first-stage decisions are evaluated across all scenarios.

The total expected cost of each approach is reported in Table 6. Under Case 2, which incorporates all flexible resources, the progressive hedging approach achieves a total expected cost that is 1.84% lower than the deterministic approach, as shown in the lower section of Table 6. This corresponds to a €267 million value of the stochastic solution (VSS). This cost difference arises as the deterministic model underestimates the required capacity by relying on average conditions and consequently depends more heavily on shortage penalties to maintain energy balance when evaluated across the full scenario set. As detailed in Table 6, the progressive hedging model recommends 62.02 GW of new generation capacity, while the deterministic model invests in only 56.89 GW, approximately 8.27% less than the progressive hedging solution. The total system shortage in the deterministic formulation is 9.26

Table 6
Results breakdown of the stochastic model and deterministic formulation.

Technology	Case 1	Case 2	Case 3
Deterministic formulation			
Generation investment (GW)	57.80	56.89	56.90
Battery (MWh)	720	450	452
PCS (MW)	341	212	216
System shortage (MWh)	105,410	105,434	105,434
Investment cost (Billion €)	6.73	6.62	6.63
Operation cost (Billion €)	7.99	7.96	7.97
Total cost (Billion €)	14.72	**14.59**	14.60
Stochastic model			
Generation investment (GW)	62.91	62.02	62.03
Battery (MWh)	1119	1229	1269
PCS (MW)	469	428	440
System shortage (MWh)	15,327	11,385	11,271
Investment cost (Billion €)	7.44	7.35	7.36
Operation cost (Billion €)	7.03	6.97	6.97
Total cost (Billion €)	**14.47**	**14.32**	14.33
Cost reduction w.r.t DF (%)	1.66	**1.84**	1.83

times greater than in the progressive hedging. Due to the heavy penalty associated with unserved energy, the shortage cost in the deterministic case is approximately €1.05 billion, whereas in the PH approach it is approximately €113.85 million, an 89.19% reduction. This is the major driver of the overall cost difference, confirming that the deterministic solution compromises generation reliability under uncertainty.

To quantify the solution quality of the proposed algorithm in terms of the true optimality gap would require solving the full problem as a single Extensive Formulation (EF), which is not possible on our hardware, since the monolithic mixed-integer model exceeds the available memory to Gurobi and an optimality gap cannot be obtained from a single solve. This intractability is, in fact, what motivates the use of the PH algorithm. To still quantify solution quality, we solved the LP relaxation of the extensive formulation of Case 2 in which all binary variables are relaxed to the continuous interval [0,1], thereby obtaining a valid though loose lower bound. The LP relaxation yields total system cost which is 1.44% less than progressive hedging. Recall that the stochastic model solved by PH outperforms the deterministic formulation by 1.84%, which indicates the algorithm achieves at least 56.6%[1] of the benefits of adopting stochastic formulation.

4.2.3. Analysis of system dispatch and demand-side flexibility resources

To compare the impacts of demand-side flexibility resources, we define three cases at the beginning of Section 4.2. The resulting investment quantities and system reliability metrics for all three cases are summarized in Table 6 and Fig. 4. We next analyze the investment and operational outcomes for various cases.

4.2.3.1. Without demand-side flexibility resources. Case 1 represents the baseline configuration, excluding all demand-side flexibility and assuming uncontrolled EV charging. It yields the highest generation investment and system shortage, as depicted in the lower section of Table 6, due to the absence of flexible resources within the capacity expansion planning framework.

The operational dispatch of Case 1 without demand-side flexibility resources is illustrated in Fig. 5(a) over a representative 6-day period (Periods 4225–4368) under the demand of scenario 03. The dispatch is dominated by renewables, with wind peaking at 28,107 MW and solar at 17,529 MW, though their variability necessitates significant thermal backup from CCGT, coal, and OCGT units during periods of low renewable output. To further illustrate the impact of BESS on shortage reduction and peak shaving, we plot the peak day (181) of the entire time horizon in Fig. 6(a). During this day the system peak reaches 41,175 MW and the BESS reaches a peak state of charge of 1219.8 MWh, operating actively and discharging up to 260 MW during shortage hours, reducing the unserved energy by 5.78% on that day alone. Though BESS contributes to reducing the unserved energy, it has no measurable impact on peak shaving. In fact, because the peak demand coincides with strong solar availability, the BESS is charging at that hour and slightly raises the peak seen by generation by about 0.51%. The majority of its operation is devoted to energy arbitrage, charging during periods of high renewable availability and discharging when renewable output declines. Across the full horizon, the remaining probability weighted unserved energy of scenario 3 of Case 1 still amounts to 6771 MWh, which the CVaR-based risk formulation retains as economically optimal rather than eliminating through additional investment.

4.2.3.2. Contribution of all demand-side flexibility resources. Case 2 introduces the full co-optimization framework, integrating all three demand-side flexibility mechanisms maintenance-based industrial scheduling, shift-flexible factory operations, and controllable EV charging alongside generation and storage investment decisions. This co-optimization reduces the total system cost by 1.04% relative to the baseline Case 1 as shown in Table 6. Correspondingly, the required generation capacity decreases by 1.41%, indicating that demand-side flexibility effectively substitutes for supply-side capacity.

The operational mechanism behind these investment savings is illustrated in Fig. 5(b) for the same representative 6-day period (Periods 4225–4368). During this high-stress period, the system dispatch remains dominated by renewables, whose variability necessitates notable thermal backup. The model schedules industrial and factory curtailment during peak hours, while flexible EV charging is co-optimized within a 24-hour window of each day. The detailed curtailment patterns during peak hours of both industries and factories across all demand scenarios within the window (Periods 4153–4704) are illustrated separately in Fig. 7. To further illustrate the combined impact of demand-side flexibility and BESS on shortage reduction and peak shaving, we plot the peak day of the entire horizon for Case 2, which coincides with the same day as in Case 1, as shown in Fig. 6(b). On this day, factory curtailment of up to 750 MW and industry curtailment of up to 498 MW persist across the stressed hours, directly offsetting peak thermal dispatch and reducing the unserved energy by about 25.72%. The system-wide peak is reduced by about 20 MW relative to Case 1 and by 248 MW (about 0.59%) relative to Case 3. BESS, by contrast, has no measurable impact on peak shaving and its operation is devoted primarily to intra-day energy arbitrage. The combined reduction in total system cost and in unserved energy during high-stress demand periods, observed in Case 2, demonstrates the value of co-optimizing flexible demand within the capacity expansion framework.

4.2.3.3. Contribution of smart EV charging. In Case 3, demand-side flexibility is restricted to industrial maintenance and work-shift scheduling, while EV charging is included without smart-charging capability. This configuration yields a total system cost only about 0.06% higher than Case 2, indicating a minor cost effect from treating EV load as inflexible. Because the operational dispatch, industrial curtailment schedules, BESS sizing, and annual unserved energy are nearly identical to those described for Case 2 in Section 4.2.3.2, a separate dispatch plot for the same high-stress window (Periods 4225–4368) is omitted, and the differences are confined to the timing of EV charging and the corresponding thermal and storage adjustments. The distinctions relative to Case 2 emerge most clearly on peak day 181, where the unserved energy is reduced by about 26.51% relative to Case 1, approximately matching the 25.72% reduction achieved in Case 2 and confirming that industrial DSM is the dominant driver of shortage reduction. However, inflexible EV charging shifts the optimizer toward larger midday BESS uptake, so BESS charges at the solar-peak hour and raises the peak

[1] This is calculated from the objective values of the different policies, i.e., $(\mathrm{DF}-\mathrm{PH})/(\mathrm{DF}-\mathrm{LP}) = (14.593-14.325)/(14.593-14.11) = 0.268/0.483 \approx 56.6\%$, where objective values are in billion €.

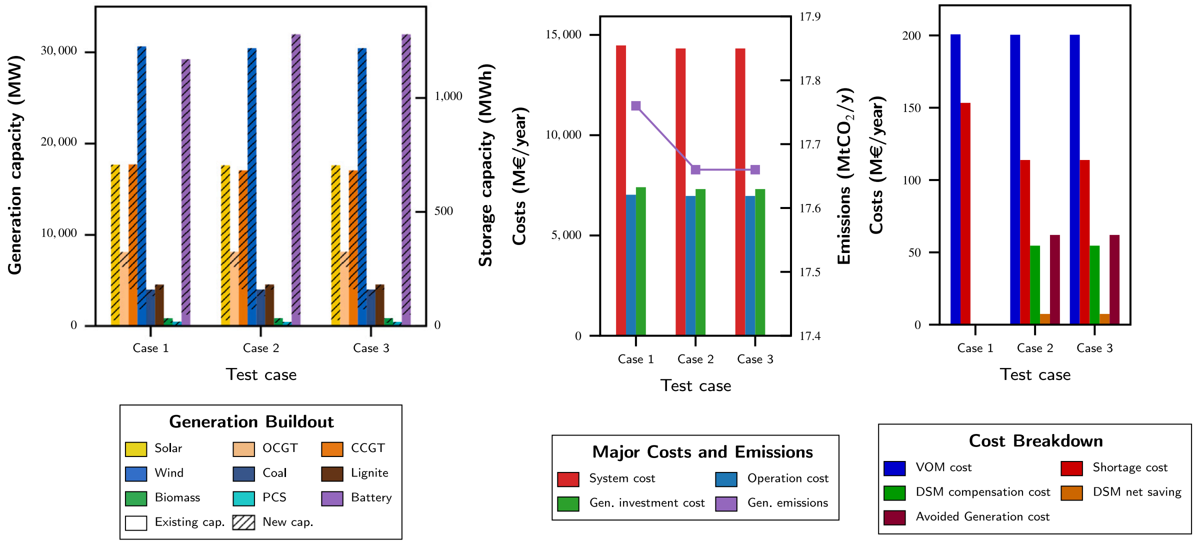

(a) Generation and storage buildout (b) Major cost and Emissions (c) Costs Breakdown

Fig. 4. (a) Generation and storage capacity buildout for each test case. Hatched regions indicate newly invested capacity, while solid regions indicate existing capacity. (b) Major cost and CO_2 emissions for each test case. System costs and emissions decrease progressively from Case 1 to Case 3, with Cases 2 and 3 additionally incurring DSM costs. (c) Major cost breakdown of each test case, including shortage cost and net savings from demand-side management.

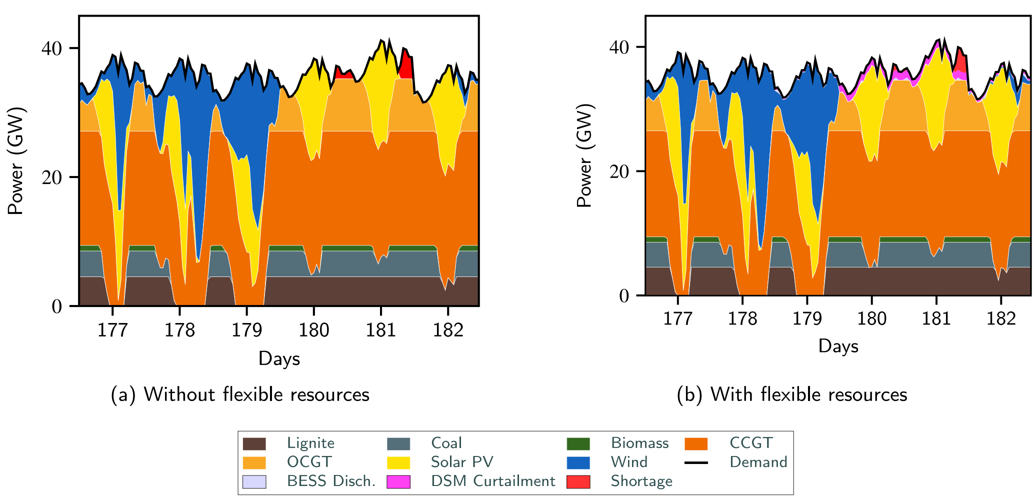

(a) Without flexible resources (b) With flexible resources

Fig. 5. Comparison of operational dispatch over a representative 6-day period (Periods 4225–4368) under scenario 03, where Fig. (a) shows Case 1 without flexible resources and Fig. (b) shows Case 2 with flexible resources.

seen by generation by about 0.61%, exceeding the 0.51% effect in Case 1, while still discharging up to 453 MW during shortage hours. Consequently, the system-wide peak in Case 3 (41,404 MW) slightly exceeds that of Case 1 (41,175 MW), whereas Case 2 achieves the lowest peak (41,155 MW). This contrast between Case 2 and Case 3 reveals a division of roles within the proposed framework, where industrial demand-side management is the dominant source of flexibility value for shortage reduction, while controllable EV charging is the mechanism responsible for peak shaving.

To check the impact of a different EV profile, a sensitivity analysis has also been performed with an alternative midday-peaked profile of the same daily energy, which changes the total system cost by only 0.034%, confirming that the results are insensitive to the profile's exact shape, which is due to the relatively lower EV penetration level.

4.2.4. Impacts of CVaR on system cost and load shedding

To examine how the shedding-risk coefficient C^{sh} and confidence level α shape the planning outcome, we solve Case 1 of the stochastic model over a grid of shedding-risk weights $C^{sh} \in \{500, 1000, 3000, 5000, 10{,}000\}$ €/MWh and confidence levels $\alpha \in \{0.60, 0.70, 0.80, 0.90, 0.95\}$, recording the resulting total system cost and expected system shortage. The analysis requires solving the model 25 times and we did not choose Case 2 due to the computational challenges, but the results from Case 1 would be advisory for Case 2. Fig. 8 reports the total cost over this (α, C^{sh}) grid. As shown in Fig. 8(a), increasing C^{sh} makes shortage in the worst scenarios more expensive, so the model invests additional generation and storage capacity, the expected system shortage is driven down, and the Value-at-Risk level l^{VaR} is consequently lowered. Over the grid the total system cost ranges from €18.78 billion down to about €14.37 billion at (α = 0.70, C^{sh} = 10,000 €/MWh). Correspondingly, the expected energy not served decreases from 538,618 to 15,327 MWh.

Fig. 8(b) isolates the effect of α. Keeping C^{sh} fixed while raising α increases the CVaR multiplier applied to the excess load shedding l^{sh+}_{ω}, making worst-case shortage more costly. The model again responds by adding generation and storage investment, so the expected shortage

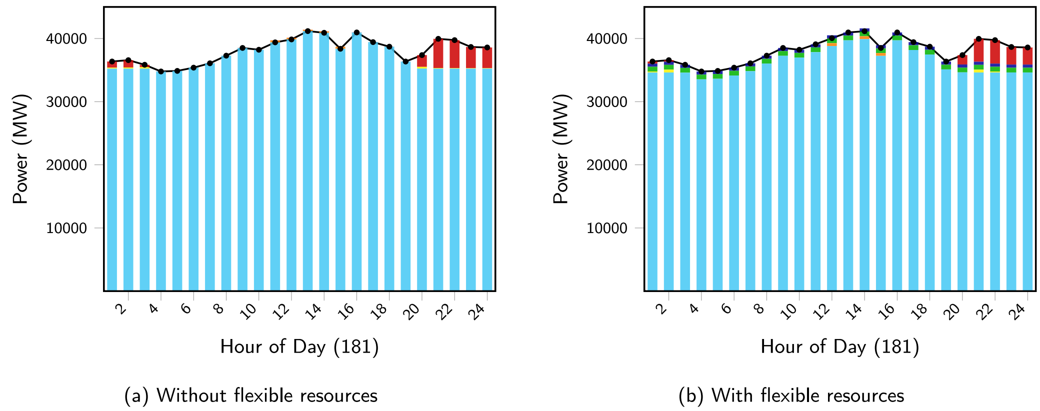

Fig. 6. Hourly dispatch on peak day 181 of the horizon: (a) Case 1 without flexible resources, (b) Case 2 with flexible resources including industrial curtailment.

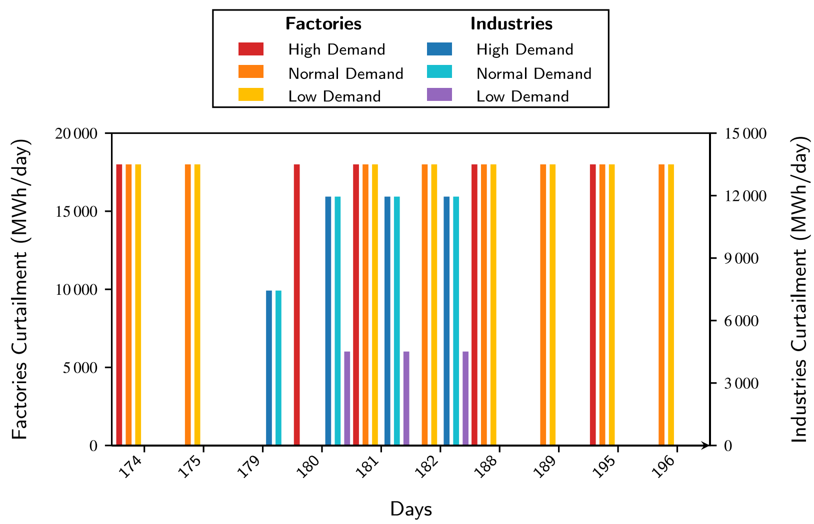

Fig. 7. Daily industrial curtailment plot in Case 2, over days 174–196.

is consistently reduced. The effect on total cost, however, depends on C^{sh}. At low weights, tightening α from 0.60 to 0.95 lowers total cost by about 9.6% at C^{sh} = 500 €/MWh, whereas at the highest weight (C^{sh} = 10,000 €/MWh) the added capacity slightly outweighs the savings and cost rises marginally by about 0.7%. Increasing both parameters jointly yields the lowest expected shortage. This trade-off makes the cost of incremental reliability explicit, allowing the planner to select (α, C^{sh}) consistent with a target adequacy level.

5. Conclusion

This paper developed a two-stage stochastic capacity expansion planning model that jointly optimizes generation investment, independently sized battery power and energy capacities, flexible electric vehicle charging, and binary industrial demand-side management scheduling under demand and electric vehicle penetration uncertainties, solving the resulting large-scale mixed-integer linear program through a Progressive Hedging decomposition with a Conditional Value-at-Risk penalty on the energy not served. Three principal findings emerge from the case studies on the Pakistani power system. First, the stochastic model produces more robust and cost-effective investment decisions, achieving a total expected cost that is 1.84% lower than the deterministic formulation, which underestimates the required capacity by relying on average conditions and depends more heavily on shortage penalties to maintain energy balance. Second, coordinating flexible demand lowers total system cost by 1.04% compared to the inflexible baseline Case 1, showing that industrial demand-side management supplies critical operational flexibility in capacity-constrained systems without additional generation investment. Third, the Progressive Hedging decomposition reaches consensus investment decisions in 31 iterations at a final primal residual of 0.4 MW, rendering a large mixed-integer linear program tractable.

Several limitations point to directions for future work. First, electric vehicle charging is currently modeled as an aggregate flexible load scaled by a fixed penetration level, incorporating home and work charging heterogeneity, driver behavior would allow more realistic

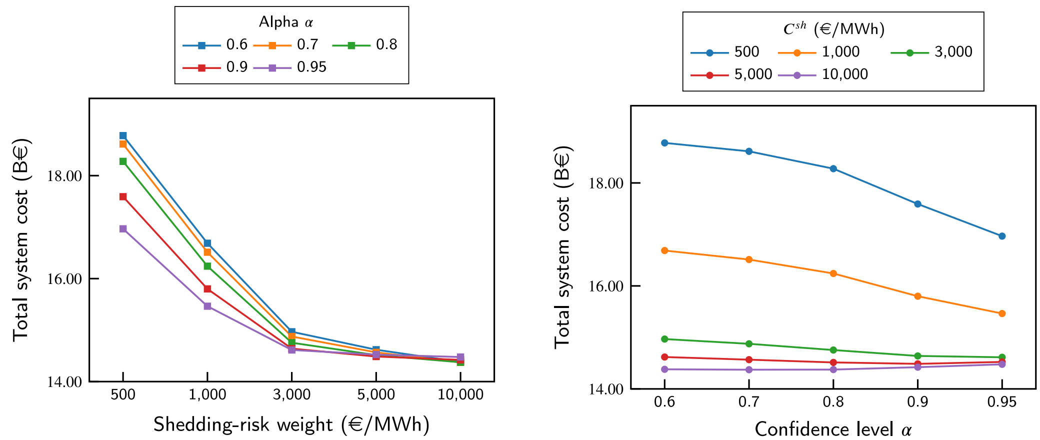

(a) Fix Alpha and varying shedding-risk weight

(b) Fix shedding-risk weight and varying Alpha

Fig. 8. Comparison of total system cost sensitivity to the CVaR confidence level α and the shedding-risk weight C^{sh}.

modeling. In addition, by considering vehicle-to-grid capability would allow electric vehicles to discharge back to the grid and provide additional flexibility and adequacy under stressed scenarios. Second, extending the industrial demand-side management formulation with start-up and shutdown costs and minimum on and off times would enable finer-grained mechanisms such as hourly load shifting in continuous processes. Finally, the single-bus (copper-plate) representation omits transmission constraints and the locational dependence of demand-side flexibility; embedding network topology and transmission capacity limits would let the locational value of demand-side management and the trade-off between generation, storage, and network investment be assessed jointly.

CRediT authorship contribution statement

Yuting Mou: Writing – review & editing, Writing – original draft, Supervision, Methodology, Investigation, Funding acquisition, Conceptualization. **Abdullah:** Writing – review & editing, Writing – original draft, Software, Methodology, Investigation, Data curation, Conceptualization.

Declaration of Generative AI and AI-assisted technologies in the writing process

During the preparation of this manuscript, the authors used large language model ChatGPT for language editing, grammatical correction, and paper organization suggestions. The authors carefully reviewed and revised the output and take full responsibility for the content of this publication.

Declaration of competing interest

The authors declare that they have no known competing financial interests or personal relationships that could have appeared to influence the work reported in this paper.

Acknowledgments

The work of Yuting Mou is supported by the National Natural Science Foundation of China under Grant No. 62403126. Abdullah gratefully acknowledges the fully funded Master's scholarship awarded by Southeast University, as well as the academic license of Gurobi used to obtain the results presented in this work.

Appendix. Nomenclature

A.1. Sets

$\mathcal{G}$	Set of generation technologies
$\mathcal{J}$	Set of battery energy storage systems
$\mathcal{N}^{\mathrm{MS}}$	Set of all maintenance and work-shift consumers
$\mathcal{N}^{\mathrm{M}}$	Set of maintenance consumers, $\mathcal{N}^{\mathrm{M}} \subset \mathcal{N}^{\mathrm{MS}}$
$\mathcal{N}^{\mathrm{S}}$	Set of work-shift consumers, $\mathcal{N}^{\mathrm{S}} \subset \mathcal{N}^{\mathrm{MS}}$
$\mathcal{T}$	Set of time periods (hours) in the planning horizon
$\mathcal{T}_w$	Set of time periods belonging to week w
$\mathcal{W}$	Set of weeks in the planning horizon
$\mathcal{D}$	Set of days in the planning horizon
$\mathcal{H}_d$	Set of hours belonging to day d
Ω	Set of uncertainty scenarios

A.2. Indices

g	Generation technology, $g \in \mathcal{G}$
j	Storage unit, $j \in \mathcal{J}$
n	Industrial consumer, $n \in \mathcal{N}^{\mathrm{MS}}$
t	Time period (hour), $t \in \mathcal{T}$
ω	Scenario, $\omega \in \Omega$
w	Week, $w \in \mathcal{W}$
d	Day, $d \in \mathcal{D}$
k	Progressive Hedging iteration

A.3. Parameters

A.3.1. Investment and fixed costs

IC_g	Annualized investment cost of generation technology g, [€/MW/yr]
FOM_g	Fixed operation and maintenance cost of generation technology g, [€/MW/yr]
$\mathrm{IC}_j^{\mathrm{PCS}}$	Annualized investment cost of power conversion system j, [€/MW/yr]
$\mathrm{FOM}_j^{\mathrm{PCS}}$	Fixed O&M cost of power conversion system j, [€/MW/yr]
$\mathrm{IC}_j^{\mathrm{BA}}$	Annualized investment cost of battery energy capacity j, [€/MWh/yr]
$\mathrm{FOM}_j^{\mathrm{BA}}$	Fixed O&M cost of battery energy capacity j, [€/MWh/yr]

A.3.2. Operational costs

MC_g	Marginal fuel cost of generation technology g, [€/MWh]
VOM_g	Variable O&M cost of generation technology g, [€/MWh]
DG_j	Degradation cost of BESS discharge, [€/MWh]
$\mathrm{VOM}_j^{\mathrm{BESS}}$	Variable O&M cost of BESS j, [€/MWh]
C_t	Penalty cost for industrial curtailment in period t, [€/MWh]

A.3.3. System and operational parameters

$\tilde{x}_g$	Existing installed capacity of generation technology g, [MW]
$\tilde{x}_j^{\mathrm{PCS}}$	Existing installed power conversion system capacity of BESS j, [MW]
$\tilde{x}_j^{\mathrm{BA}}$	Existing installed battery energy capacity of BESS j, [MWh]
$\rho_{g,t}$	Availability factor of generation technology g in period t, dimensionless
EF_g	CO_2 emission factor of generation technology g, [tCO_2/MWh]
$D_{t,\omega}$	System electricity demand in period t under scenario ω, [MW]
P_ω	Probability of scenario ω, dimensionless

A.3.4. BESS parameters

η^{ch}	Charging efficiency, dimensionless
η^{dis}	Discharging efficiency, dimensionless
E_0	Initial and daily reference state of charge, [MWh]

A.3.5. DSM parameters

P_n	Rated power consumption of industrial consumer n, [MW]
D_n^{M}	Required maintenance shutdown duration of consumer $n \in \mathcal{N}^{\mathrm{M}}$, [days]
D_n^{S}	Required weekly off-day duration of consumer $n \in \mathcal{N}^{\mathrm{S}}$, [days]

A.3.6. EV parameters

ϕ_ω	EV penetration fraction in scenario ω, [%]
λ_ω	Demand scaling factor in scenario ω, dimensionless
P_ω^{EV}	Maximum EV charging power in scenario ω, [MW]
$\alpha_{h(t)}^{\mathrm{EV}}$	EV charging availability factor at hour-of-day $h(t)$, dimensionless
$\bar{\alpha}^{\mathrm{EV}}$	Average daily EV availability factor, dimensionless
$h(t)$	Hour-of-day mapping, $h(t) = ((t-1) \bmod 24) + 1$

A.3.7. Risk (CVaR) parameters

C^{sh}	Shedding-risk coefficient; penalty weight on the CVaR of energy not served, [€/MWh]
α	CVaR confidence level (tail probability $1-\alpha$), dimensionless

A.3.8. Progressive hedging parameters

ρ_g	Penalty parameter for generation technology g
ρ_j^{PCS}	Penalty parameter for PCS capacity of BESS j
ρ_j^{BA}	Penalty parameter for battery capacity of BESS j
ρ^{VaR}	Penalty parameter for the Value-at-Risk variable
ρ_{base}	Base penalty scaling factor
ϵ_{abs}	Absolute primal residual tolerance, [MW/MWh]
ϵ_{rel}	Relative primal residual tolerance, [%]
ϵ_{obj}	Objective change tolerance, [%]
ϵ_{dev}	Maximum first-stage deviation tolerance, [MW/MWh]
$K_{\max}$	Maximum number of PH iterations

A.4. Decision variables

A.4.1. First-stage (investment) variables

x_g	New capacity of generation technology g, [MW]
x_j^{PCS}	New power conversion system capacity of BESS j, [MW]
x_j^{BA}	New battery energy capacity of BESS j, [MWh]

A.4.2. Second-stage (operational) variables

$p_{g,t,\omega}$	Power output of generation technology g in period t under scenario ω, [MW]
$p_{j,t,\omega}^{\mathrm{ch}}$	BESS j charging power in period t under scenario ω, [MW]
$p_{j,t,\omega}^{\mathrm{dis}}$	BESS j discharging power in period t under scenario ω, [MW]
$e_{j,t,\omega}$	State of charge of BESS j in period t under scenario ω, [MWh]
$p_{t,\omega}^{\mathrm{EV}}$	EV charging power in period t under scenario ω, [MW]
$\mu_{n,t,\omega}$	Binary variable, 1 if consumer n is curtailed in period t under scenario ω
$v_{n,t,\omega}$	Binary variable, 1 if consumer n starts curtailment in period t under scenario ω
$z_{n,t,\omega}$	Binary variable, 1 if consumer n ends curtailment in period t under scenario ω
$l_{t,\omega}^{\mathrm{sh}}$	Involuntary load shedding in period t under scenario ω, [MW]

A.4.3. Risk (CVaR) variables

l^{VaR}	Value-at-Risk of load shedding; first-stage (non-anticipative) consensus variable, [MWh]
$l_\omega^{\mathrm{sh}+}$	Load shedding in excess of the Value-at-Risk in scenario ω, [MWh]

A.4.4. Progressive hedging variables

$x_{g,\omega}$	Scenario-specific generation capacity of technology g in scenario ω, [MW]
$x_{j,\omega}^{\mathrm{PCS}}$	Scenario-specific PCS capacity of BESS j in scenario ω, [MW]
$x_{j,\omega}^{\mathrm{BA}}$	Scenario-specific battery capacity of BESS j in scenario ω, [MWh]
l_ω^{VaR}	Scenario-specific (local copy of the) Value-at-Risk in scenario ω, [MWh]
$\bar{x}_g^k$	Consensus generation capacity of technology g at iteration k, [MW]
$\bar{x}_j^{\mathrm{PCS},k}$	Consensus PCS capacity of BESS j at iteration k, [MW]

$\bar{x}_j^{\mathrm{BA},k}$	Consensus battery capacity of BESS j at iteration k, [MWh]
$\bar{l}^{\mathrm{VaR},k}$	Consensus Value-at-Risk at iteration k, [MWh]
f_ω^k	Augmented Lagrangian objective value of scenario ω at iteration k, [€]
r^k	Primal residual at iteration k, [MW/MWh]
r_{rel}^k	Relative primal residual at iteration k, [%]

Data availability

Data will be made available on request.

References

[1] Kazmi H, Mehmood F, Tao Z, Riaz Z, Driesen J. Electricity load-shedding in Pakistan: unintended consequences, opportunities and policy recommendations. TIDEE: TERI Inf Dig Energy Environ 2020;19(2):183.

[2] Timilsina G, Steinbuks J. Economic costs of electricity load shedding in Nepal. Renew Sustain Energy Rev 2021;146:111112.

[3] Hunt JD, Stilpen D, de Freitas MAV. A review of the causes, impacts and solutions for electricity supply crises in Brazil. Renew Sustain Energy Rev 2018;88:208–22.

[4] Heggie A, Eager D, McKinnon K, Van Der Weijde AH. Power rationing in a long-term power shortage. Energy Policy 2018;121:202–10.

[5] Abdullah, Mou Y. Capacity expansion planning with flexible large-scale load scheduling. In: 2026 38th Chinese control and decision conference. CCDC, 2026, p. 4333–8. http://dx.doi.org/10.1109/CCDC69976.2026.11560163.

[6] Amirifard M, Sinton RA, Kurtz S. How demand-side management can shape electricity generation capacity planning. Util Policy 2024;88:101748.

[7] Roh JH, Shahidehpour M, Wu L. Market-based generation and transmission planning with uncertainties. IEEE Trans Power Syst 2009;24(3):1587–98.

[8] Lin J, Ma J, Zhu J, Cui Y. Short-term load forecasting based on lstm networks considering attention mechanism. Int J Electr Power Energy Syst 2022;137:107818.

[9] Kim D, Ryu H, Lee J, Kim K-K. Balancing risk: Generation expansion planning under climate mitigation scenarios. European J Oper Res 2022;297(2):665–79.

[10] Ahmad H, Jamil F. Investigating power outages in Pakistan. Energy Policy 2024;189:114117.

[11] Mo B, Hegge J, Wangensteen I. Stochastic generation expansion planning by means of stochastic dynamic programming. IEEE Trans Power Syst 1991;6(2):662–8.

[12] Birge JR, Louveaux F. Introduction to stochastic programming. New York, NY: Springer; 1997.

[13] Cho S, Li C, Grossmann IE. Recent advances and challenges in optimization models for expansion planning of power systems and reliability optimization. Comput Chem Eng 2022;165:107924. http://dx.doi.org/10.1016/j.compchemeng.2022.107924.

[14] Go RS, Munoz FD, Watson J-P. Assessing the economic value of co-optimized grid-scale energy storage investments in supporting high renewable portfolio standards. Appl Energy 2016;183:902–13.

[15] Yang Y, Mou Y, Li J, Wang B, Li C, Yang X. Impact of capacity market mechanism on high renewable penetration systems with long-term energy storage. Energy Convers Econ 2025;6(5):295–307.

[16] Radmanesh H, Barkam E. Robust co-planning of transmission expansion and merchant energy storage investments considering long-and short-term uncertainties. Int J Electr Power Energy Syst 2024;160:110062.

[17] Piansky R, Stinchfield G, Kody A, Molzahn DK, Watson J-P. Long duration battery sizing, siting, and operation under wildfire risk using progressive hedging. Electr Power Syst Res 2024;235:110785.

[18] Marañón-Ledesma H, Tomasgard A. Analyzing demand response in a dynamic capacity expansion model for the European power market. Energies 2019;12(15):2976.

[19] Wei H, Ma M, Jiang H, Capuder T, Teng F, Strbac G, et al. Generation and transmission expansion planning incorporating economically feasible heterogeneous demand-side resources. Appl Energy 2025;381:125067.

[20] Oderinwale T, Papadaskalopoulos D, Ye Y, Strbac G. Investigating the impact of flexible demand on market-based generation investment planning. Int J Electr Power Energy Syst 2020;119:105881.

[21] Karimi H, Heydarian-Forushani E, Mehri S, Salman M, Ghandour R, Zayyani H. A bi-level multi-energy scheduling model for virtual power plants in competitive market environment. Electr Power Syst Res 2026;254:112612.

[22] Karimi H, Heydarian-Forushani E. A multi-objective bi-level framework to model distribution system operator's behavior in the wholesale and local transactive markets. Energy 2024;312:133695.

[23] Usman R, Mirzania P, Alnaser SW, Hart P, Long C. Systematic review of demand-side management strategies in power systems of developed and developing countries. Energies 2022;15(21):7858.

[24] Xiao Y, Mou Y, Pan B, Yang M. The design of a time-of-use tariff with a demand charge for residential electric vehicle charging posts. Util Policy 2025;97:102078. http://dx.doi.org/10.1016/j.jup.2025.102078.

[25] Da Costa LC, Thomé FS, Garcia JD, Pereira MVF. Reliability-constrained power system expansion planning: A stochastic risk-averse optimization approach. IEEE Trans Power Syst 2020;36(1):97–106.

[26] Pecci F, Jenkins JD. Regularized Benders decomposition for high performance capacity expansion models. IEEE Trans Power Syst 2025;40(4):3105–16.

[27] Zampara M, Ávila D, Papavasiliou A. Capacity expansion planning under uncertainty subject to adequacy constraints. IEEE Trans Power Syst 2026. http://dx.doi.org/10.1109/TPWRS.2026.3707026.

[28] Rockafellar RT, Wets RJ-B. Scenarios and policy aggregation in optimization under uncertainty. Math Oper Res 1991;16(1):119–47.

[29] Watson J-P, Woodruff DL. Progressive hedging innovations for a class of stochastic mixed-integer resource allocation problems. Comput Manag Sci 2011;8(4):355–70.

[30] Kaisermayer V, Muschick D, Horn M, Gölles M. Progressive hedging for stochastic energy management systems: The mixed-integer linear case. Energy Syst 2021;12(1):1–29.

[31] Munoz FD, Watson J-P. A scalable solution framework for stochastic transmission and generation planning problems. Comput Manag Sci 2015;12(4):491–518.

[32] Zuluaga TV, Musselman A, Watson J-P, Oren SS. Parallel computing for power system climate resiliency: Solving a large-scale stochastic capacity expansion problem with MPI-SPPy. Electr Power Syst Res 2024;235:110720.

[33] Rockafellar RT, Uryasev S. Optimization of conditional value-at-risk. J Risk 2000;2(3):21–41.

[34] National Transmission and Dispatch Company Limited (NTDC). National transmission and dispatch company. 2023, available: http://www.ntdc.com.pk/.

[35] National Electric Power Regulatory Authority (NEPRA). Quarterly tariff indexation reports. Tech. rep., Islamabad, Pakistan; 2020–2024, available: https://www.nepra.org.pk/.

[36] National Transmission and Dispatch Company Limited (NTDC). Indicative generation capacity expansion plan. Tech. rep., 2021, available: https://fpcci.org.pk/wp-content/uploads/2021/11/IGCEP-2021.pdf.

[37] Artelys. Data from Artelys studies. 2022, available: https://www.artelys.com/.

[38] Koffi B, Cerutti A, Duerr M, Iancu A, Kona A, Janssens-Maenhout G. CoM default emission factors for the member states of the European union. European Commission, Joint Research Centre (JRC); 2017.

[39] NASA Langley Research Center (LaRC) POWER Project. POWER data access viewer. 2024, available: https://power.larc.nasa.gov/data-access-viewer/.

[40] International Renewable Energy Agency (IRENA). Renewable power generation costs in 2022. Tech. rep., 2023, available: https://www.irena.org/-/media/Files/IRENA/Agency/Publication/2023/Aug/IRENA_Renewable_power_generation_costs_in_2022.pdf.

[41] IEA Photovoltaic Power Systems Programme. Performance of photovoltaic (PV) systems: modelling and monitoring. Tech. rep, vol. 13, IEA PVPS Task; 2019.

[42] Raza MA, Khatri KL, Israr A, Haque MIU, Ahmed M, Rafique K, et al. Energy demand and production forecasting in Pakistan. Energy Strategy Rev 2022;39:100788.

[43] Mou Y, Wang B, Shen Z. An optimization scheme for designing power rationing schedules in a long-term power shortage. Electr Power Syst Res 2023;225:109816.